



Rare earth-doped Ni/MgAl₂O₄ catalysts prepared via a one-step sol–gel method for steam reforming of volatile organic solvents at low temperatures

Feng Lin ^a, Xiangwei Ma ^a, Zezhi Chen ^{a,*}, Huijuan Gong ^{a,b,**}, Mingze Xu ^a

^a State Key Laboratory of Pollution Control and Resource Reuse, School of Environment, Nanjing University, 210023 Nanjing, PR China

^b Center of Material Analysis, Nanjing University, 210023 Nanjing, PR China



ARTICLE INFO

Keywords:

Volatile organic solvents
Catalytic steam reforming
Rare earth doping
Ni/MgAl₂O₄
Low temperature

ABSTRACT

To develop efficient steam reforming catalysts that are widely applicable to various volatile organic solvents under low temperatures, rare earth (La, Ce or Pr)-doped Ni/MgAl₂O₄ were prepared via a novel one-step sol–gel method. Through various characterizations and DFT calculations, it demonstrated that the rare earths not only improved the catalyst structure, but also promoted the dispersion, electron density and d-band center of Ni. Consequently, all the rare earth-doped Ni/MgAl₂O₄ catalysts exhibited higher catalytic activity in steam reforming of different volatile organic solvents than the Ni/MgAl₂O₄ in 500–550 °C. Thereinto, the 10Ni–2La/MgAl₂O₄ performed the best, achieving a conversion efficiency of 97.3% at 550 °C for the mixture of toluene, acetone, tetrahydrofuran, and n-hexane. The outstanding performance of Ni-La/MgAl₂O₄ catalyst arises from the structural compatibility between low-spin La atom and Ni cluster, which enables La to modify Ni dispersion and electronic structure more significantly than Ce or Pr.

1. Introduction

Volatile organic solvents, such as acetone, tetrahydrofuran, toluene and n-hexane, are widely utilized as reaction media or agents for purification, cleaning and extraction in the pharmaceutical and chemical industries [1]. The high volatility renders them susceptible to being released as waste gases, resulting in significant solvent loss and severe environmental consequences [1]. It was estimated that the annual emissions of volatile organic solvents from industrial production in China or the United States are tens of millions of tons [2,3]. Adsorption, absorption, membrane separation, and condensation are commonly employed in the industries for recovering solvent waste gases [4]. However, reusing the recovered solvents is hindered by their multi-component nature, necessitating cumbersome and expensive separation processes. Additionally, pharmaceutical industries frequently encounter azeotropes and near-boiling mixtures (such as acetone-tetrahydrofuran and water-tetrahydrofuran) that pose challenges for separation [5]. Therefore, many factories would rather incinerate the recovered solvents as waste than reuse them [6]. High-temperature incineration is characterized by high energy

consumption and waste of solvent resources. Thereby, there is an urgent need for environmentally friendly and cost-effective methods to dispose of the recovered solvents.

An innovative strategy for reuse of the recovered solvents as resource was proposed in our recent study [7]. That is converting the recovered solvents into gas fuel (H₂, CO and CH₄) via catalytic steam reforming, and then the gas fuel is used for power generation in internal combustion engines. The feasibility of this strategy was validated by means of thermodynamic calculations. Besides, catalytic steam reforming experiments were conducted with toluene, acetone and tetrahydrofuran and their mixture as the simulated recovered solvents, and a three-dimensional macro-porous (3DOM) Ni–Pt/Ce_{0.8}Zr_{0.2}O₂ as the catalyst. Results demonstrated that the solvent conversion efficiency ranged from 90.82% to 99.52% at 600 °C. The lower heating value (LHV) of gas fuel was in the range of 4.24–6.38 MJ/m³. The net electricity generated from treating 1 kg/h of solvents ranges from 0.80 to 1.44 kWh, and the net profit can range between 3.05 and 3.34 €. While, the disposal cost for conventional incineration is around 0.92 € per kg of solvents [7]. Obviously, this resource reuse strategy for the recovered solvents is believed to have great prospect in industrial applications.

* Corresponding author.

** Corresponding author at: State Key Laboratory of Pollution Control and Resource Reuse, School of Environment, Nanjing University, 210023 Nanjing, PR China.

E-mail addresses: chenzzg@nju.edu.cn (Z. Chen), gonghj@nju.edu.cn (H. Gong).

The steam reforming catalyst is the key to this strategy to ensure efficient and stable conversion of the various solvents into gas fuel. The 3DOM Ni–Pt/Ce_{0.8}Zr_{0.2}O₂ catalyst used has been proved applicability [7]. However, such catalyst has certain limitations. The use of Pt suggests a relatively high cost of catalyst, and the preparation process is cumbersome. Besides, mechanical strength of the obtained catalyst is unsatisfactory. These issues curtail the applicability of this catalyst in industrial applications.

The objective of this study is to develop a cost-effective steam reforming catalyst with excellent low-temperature activity, wide adaptability, and good stability for the common solvents. It is worth emphasizing that relatively low steam reforming temperatures (500–600 °C) are significant in reducing energy consumption and catalyst sintering. To date, little research has focused on low-temperature activity of steam reforming catalysts [8]. Ni-based catalysts are the most widely studied and used steam reforming catalysts. Ni component is generally loaded onto the support, and functions by cleaving C–C/H–C/O bonds within organic molecules [9–11]. Suitable support materials promote the dispersion of Ni, which is crucial for augmenting its catalytic activity and durability against carbon deposition and sintering [12]. Among the various supports, MgAl₂O₄ spinel exhibited excellent ability in dispersing Ni. Takehira et al. found that the dispersion of Ni on MgAl₂O₄ surface (19.7%) was significantly higher than that on γ-Al₂O₃ (8.9%), α-Al₂O₃ (3.5%), and MgO (1.0%) [13]. Trane-Restrup et al. reported that the smaller NiO particles were obtained on MgAl₂O₄ support (4 nm) compared to those on CeO₂ (10 nm) and Ce_{0.6}Zr_{0.4}O₂ (28 nm), which accounted for the higher activity and coking resistance of Ni/MgAl₂O₄ catalyst for steam reforming ethanol [14]. It is noteworthy that a one-step sol-gel method for synthesizing Ni/MgAl₂O₄ was firstly proposed in our previous study [15]. This approach is simpler, more time-efficient, and the resulting Ni/MgAl₂O₄ catalyst exhibited superior specific surface area and Ni dispersion compared to other methods commonly used in literature (see Table S1 in Supplementary Materials). In the preliminary test, such Ni/MgAl₂O₄ catalyst with 20 wt% of Ni loading demonstrated a toluene steam reforming efficiency of 84.5% at 600 °C [15]. In short, the Ni/MgAl₂O₄ is expected to be a promising catalyst candidate for steam reforming various volatile organic solvents.

Adding promoters is an approach to improve catalyst performance. Rare earths might be a kind of potential cost-effective promoter for Ni/MgAl₂O₄ catalyst. Fard et al. discovered that the Ce dopant could refine Ni particles on MgAl₂O₄ support, which increased propane steam reforming activity and mitigated carbon deposition [16]. Park et al. found that La modification promoted the dispersion of Ni by improving its interaction with MgAl₂O₄ support, and the catalyst maintained high Ni dispersion even after being aged at 900 °C for 50 h [17]. Moreover, some researchers reported that rare earths could transfer electrons to Ni atoms. In LaNi₅ alloy, Ni atom acquired 0.15–1.50 electrons from surrounding La atoms through La 5d–Ni 3d orbital interaction [18,19]. Similarly, Li et al. reported that Ce dopant in Ce–Ni/SBA-15 catalyst facilitated electron transfer to Ni by inducing a valence change from Ce³⁺ to Ce^{δ+} ($\delta > 3$) [20]. Electron-rich Ni would exhibit a stronger electron-donating ability, which is advantageous for the adsorption of solvent molecules and activation of the corresponding chemical bonds [21,22].

Based on the discussion above, we supposed that rare earth (La, Ce or Pr)-doped Ni/MgAl₂O₄ catalysts might be a candidate to meet the objective of this study. Since the one-step sol-gel method to prepare Ni/MgAl₂O₄ catalyst showed several advantages compared with other methods, the dope of different rare-earths (La, Ce or Pr) into Ni/MgAl₂O₄ catalyst were tried via the one-step sol-gel method for the first time in this study. The obtained rare earth-doped Ni/MgAl₂O₄ catalysts were tested the catalytic conversion performance in the steam reforming of typical volatile organic solvents of different structures. The experimental results demonstrated that the rare earth-doped Ni/MgAl₂O₄ showed obvious catalytic activity improvement compared to the non-

doped catalyst in 500–550 °C. Thereinto 10Ni-2La/MgAl₂O₄ catalyst exhibited the best performance, with a reforming conversion efficiency of 97.3% for the mixture of toluene, acetone, tetrahydrofuran, and n-hexane at 550 °C. After 10 h of steam reforming reaction, the carbon deposition rate was only 0.095 mg/(h·g catalyst). Characterizations and DFT calculations revealed the modulation effect of rare earth dopants on the electronic structure of Ni (valence electron density and d-band center), and the mechanism underlying the superiority of La dopant was also explicated. These findings are expected to be a valuable addition to the current understanding of rare earth doping behavior.

2. Methods

2.1. Catalyst preparation

Referring to reference [15], and as shown in Fig. 1a, the rare earth-modified Ni/MgAl₂O₄ catalyst was synthesized via the one-step sol-gel method. For example, to prepare the catalyst with a Ni loading of 10 wt% and a La doping of 2.0 wt% (10Ni-2La/MgAl₂O₄), 9.276 g of Al(NO₃)₃•9 H₂O, 3.172 g of Mg(NO₃)₂•6 H₂O, 0.991 g of Ni(NO₃)₂•6 H₂O, and 0.124 g of La(NO₃)₃•6 H₂O were dissolved in 95 mL of ethanol. After that, 31 mL of propylene oxide (C₃H₆O) was added to the solution. The mixture was continuously stirred for around 10 min and a gel was generated. The gel was dried at 85 °C for 12 h, and finally calcined at 700 °C for 3 h (heating rate of 5 °C/min) in air. When adjusting the loading capacity of Ni or rare earth, the amount of ethanol and C₃H₆O was maintained at a ratio of ethanol/(Mg²⁺+Al³⁺+Ni²⁺+rare earth ions) = 40 mol/mol and C₃H₆O/(Mg²⁺+Al³⁺+Ni²⁺+ rare earth ions) = 11 mol/mol.

2.2. Catalytic steam reforming experiment

As shown in Fig. 1b, the catalytic steam reforming experiments were carried out in a fixed-bed quartz tubular reactor. Catalyst sample (powder, 0.5 g) mixed with quartz sand (40–60 mesh, 2 g) was loaded in the reactor, followed by reduction with 28% H₂/N₂ stream (140 mL/min) at 750 °C for 2 h. The stable production of steam and gaseous organic solvents relied on a custom-built generator, equipped with a liquid injection pump and pre-heater featuring temperature control. The pre-heater temperature was set to 5 °C below the boiling point of the targeted solvent. For the solvent mixture, the temperature setting was the same as for toluene. The injection rate was maintained at a constant value of 0.018 mol/h for toluene, acetone, tetrahydrofuran, n-hexane and their mixture (with each solvent having a molar ratio of 1:1:1:1). The injection rate of deionized water was determined by the injection speed of solvent, i.e. the molar ratio of water to carbon of solvent (S/C) was 3 mol/mol. N₂ (100 mL/min) controlled by a mass flow controller carried steam and gaseous solvent into the reactor. After a 45-minute stabilization period at the setting temperature (500, 550, or 600 °C) in each experiment, the non-condensable product gases were collected in a gas sampling bag and subsequently analyzed by an external standard method using a Thermo Trace 1310 gas chromatograph equipped with a thermal conductivity detector. The solvent conversion efficiency (η) was determined using the following equation:

$$\eta(\%) = \frac{(n_{CO} + n_{CO_2} + n_{CH_4})}{n_{solvent}} \times 100\% \quad (1)$$

in which n_{CO}, n_{CO₂} and n_{CH₄} denoted the molar flow rate of CO, CO₂ and CH₄ in product gas, respectively, and n_{solvent} represented the molar flow rate of carbon atoms of the injected solvent [8,23].

2.3. Characterizations

The reduced catalysts (reduction condition was the same as steam reforming experiment) were characterized by N₂ adsorption-desorption isotherms at 77 K on a JW-BK122W static N₂ adsorption system (JWGB

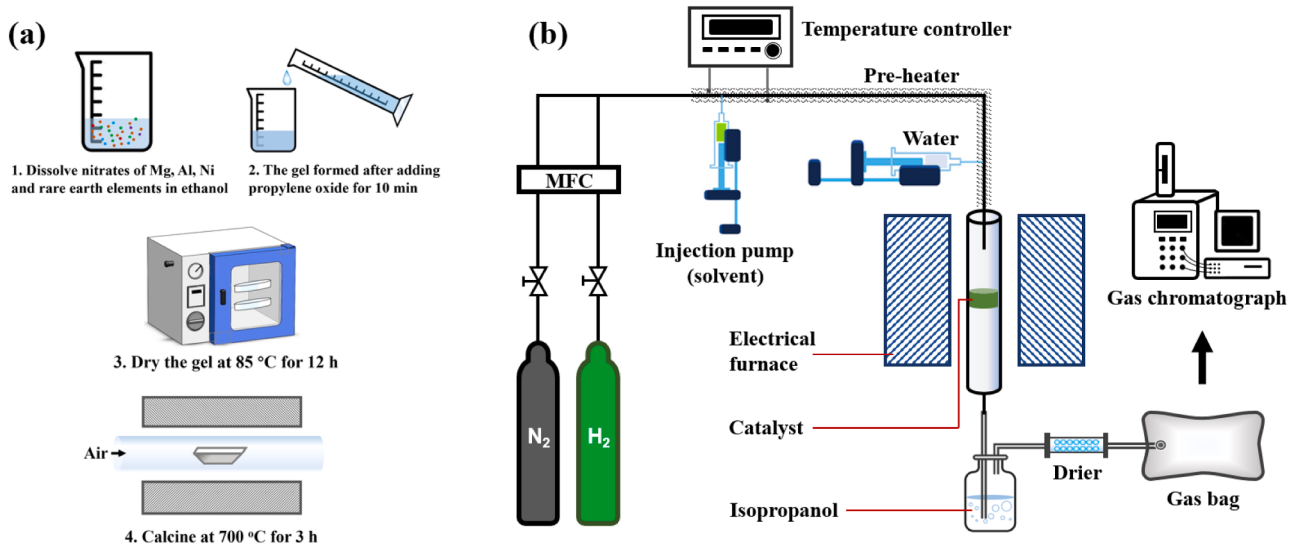


Fig. 1. Schematic illustrations of (a) the one-step sol-gel method and (b) the experimental device for catalytic steam reforming (MFC, mass flow controller).

Science and Technology Company, China). Prior to the measurement, each sample was degassed under vacuum at 150 °C for 8 h. The specific surface was calculated based on the Brunauer-Emmett-Teller (BET) standard equation, and the Barrett-Joyner-Halenda (BJH) model was used to calculate the porous parameters related to the mesoporous texture.

The crystalline structures of the reduced catalysts were characterized by powder X-ray diffraction (XRD). It was conducted on a X'TRA diffractometer (ARL, Switzerland) using a Cu $\kappa\alpha$ radiation source and a NaI (TI) scintillation detector. Scans were performed in a 20 range from 10° to 90°, with the step of 0.02° and the scan rate of 5 °/min.

H_2 -temperature programmed reduction (H_2 -TPR) and CO_2 -temperature programmed desorption (CO_2 -TPD) were performed on an AutoChem 2920 apparatus equipped with a thermal conductivity detector. The unreduced and reduced catalysts were used for H_2 -TPR and CO_2 -TPD, respectively. In H_2 -TPR experiment, after being pretreated at 300 °C for 30 min in He flow at 30 mL/min, the 0.1 g of catalyst sample was reduced in 10 vol% H_2 /Ar at 30 mL/min accompanied by temperature rising from 50 °C to 850 °C at a rate of 10 °C/min. In CO_2 -TPD experiment, 0.1 g of sample was pretreated at 300 °C for 30 min in He flow at 30 mL/min. Then, the catalyst sample was cooled down to 50 °C and exposed to 10 vol% CO_2 /He at 30 mL/min for 1 h. The desorption of CO_2 was performed by heating from 50 °C to 600 °C at 5 °C/min in He flow at 30 mL/min.

X-ray photoelectron spectroscopy (XPS) analysis of the reduced catalysts were conducted on a PHI 5000 VersaProbe (UIVAC-PHI, Japan) equipped with a hemispherical analyzer. A monochromatic Al $K\alpha$ ($h\nu = 1486.6$ eV) X-ray source was operated at 15 kV. The binding energy was calibrated using the carbonaceous C 1 s line at 284.8 eV as reference.

Carbon deposition on the used catalyst was investigated by thermogravimetric (TG) analysis on an SDT 650 (Waters Corporation, USA) synchronous thermal analyzer. The sample was heated from room temperature to 800 °C at a heating rate of 10 °C/min in air (50 mL/min).

2.4. Theoretical calculations

The spinel $MgAl_2O_4(111)$ -c(1 × 1) periodical slab was constructed to simulate support substrate. The periodical slab contained eight atomic layers and a vacuum space of 15 Å, in which only the bottom Mg and Al atoms were fixed to their bulk position. Ni_4 cluster was deposited on the outmost surface of $MgAl_2O_4(111)$ to simulate $Ni/MgAl_2O_4$. After testing for different Ni_4 structures, it was proved that Ni_4 cluster with pyramidal

structure was the most stable. The rare earth-doped catalyst model was constructed by replacing a Ni atom in cluster with a rare earth atom.

The spin-polarized density functional theory (DFT) calculations were performed using Vienna ab initio simulation program (VASP). Generalized gradient approximation (GGA) with Perdew-Burke-Ernzerh (PBE) was used as exchange-correlation functional. The projector-augmented wave (PAW) method was utilized to describe the electron-ion interactions. The cutoff energy for plane-wave basis set was 450 eV and Brillouin zone was sampled using a $4 \times 4 \times 2$ Monkhost-Pack grid. The computational parameters have been validated through tests (see Fig. S1 in Supplementary Materials). The convergence criterium of energy and force was 1×10^{-6} eV and 0.02 eV/Å, respectively. Considering the strong Coulomb interaction of electrons in Ni 3d and rare earth 4 f orbitals, the Hubbard U parameter was introduced and set for 5.0 eV for Ni 3d, La 4 f, Ce 4 f, Pr 4 f [23]. The d-band center of occupied Ni 3d orbital (ε_{Ni}) was determined by taking the centroid of the projected density of states (pDOS) relative to Fermi energy:

$$\varepsilon_{Ni} = \left(\int eN(e)de \right) / \left(\int N(e)de \right) \quad (2)$$

in which the integrated domain was $-\infty$ to Fermi energy [24]. The ab initio molecular dynamics (AIMD) simulations were conducted under a constant volume and temperature (NVT) ensemble using VASP program. Each AIMD simulation was performed at 550 °C using a Nose-Hoover thermostat chain with a time step of 1 fs.

3. Result and discussion

3.1. Performance of the catalysts in steam reforming of toluene

To determine the optimal Ni loading amount, a series of $Ni/MgAl_2O_4$ catalysts with 5, 10, 15 and 20 wt% of Ni were prepared, denoted as 5Ni/MgAl, 10Ni/MgAl, 15Ni/MgAl, and 20Ni/MgAl, respectively. The presence of a benzene ring in toluene molecule makes it more difficult to reform compared with the other three solvents. Thus, toluene was chosen to evaluate the steam reforming activity of the $Ni/MgAl_2O_4$ catalysts with different Ni loading amounts at different temperature. As shown in Fig. 2a, the optimal Ni loading of $Ni/MgAl_2O_4$ catalyst is 10 wt %. Excessive loading (15–20 wt%) might aggravate Ni component agglomeration, leading to decreased catalytic activity [23]. Furthermore, the catalytic performance of 10Ni/MgAl doped with 0.5–3 wt% of La, Ce, and Pr (denoted as 10Ni-(0.5–3) rare earth/MgAl) was evaluated, and the results are shown in Fig. 2b, c, and d correspondingly. Overall,

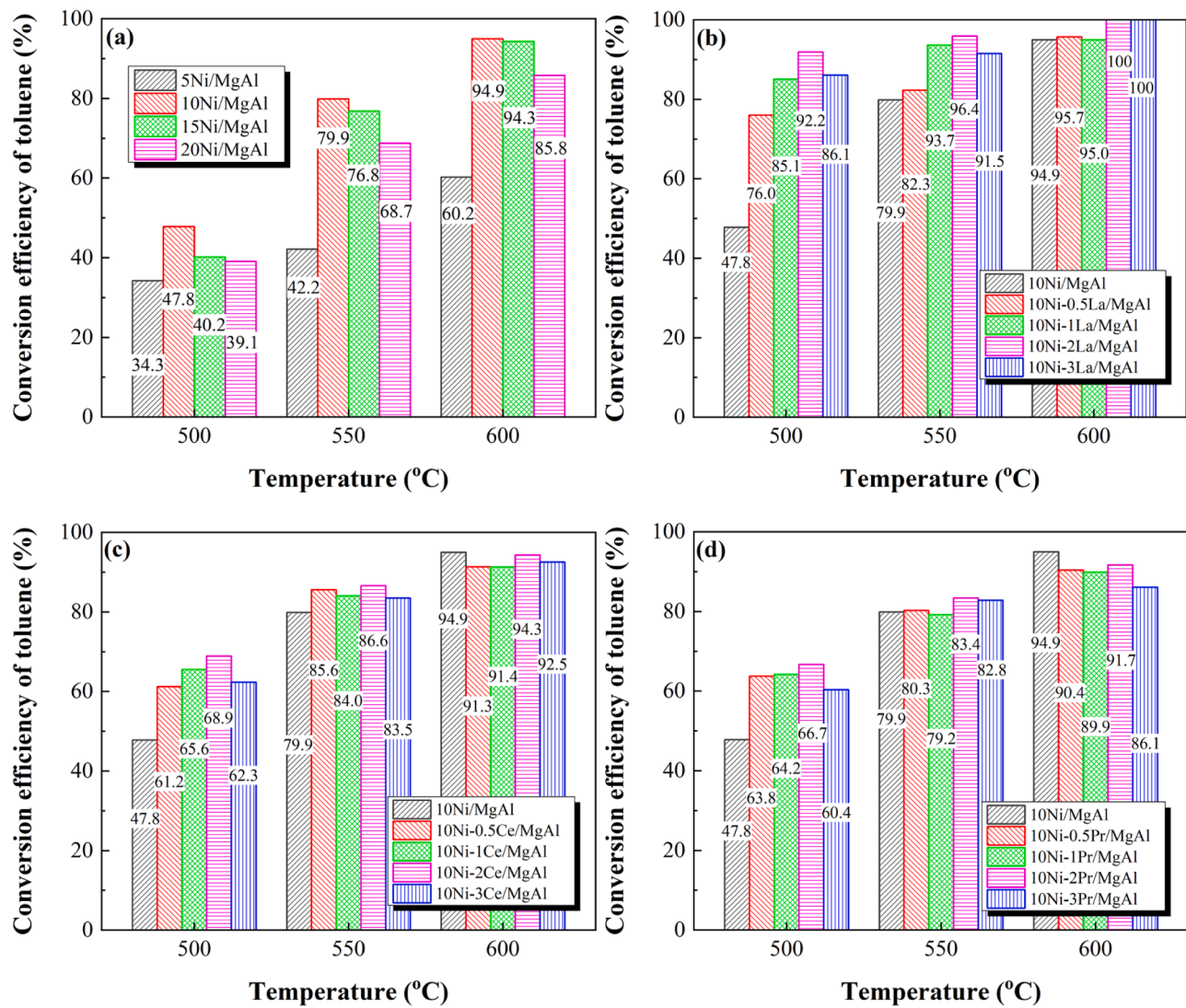


Fig. 2. Steam reforming of toluene over $\text{Ni}/\text{MgAl}_2\text{O}_4$ (a) with different Ni loading, (b, c, d) with different amount of La, Ce, Pr dopants.

doping rare earth enhanced the toluene conversion efficiency in relatively low temperatures (500–550 °C). The optimal doping amount for all the three rare earths were 2.0 wt% Insufficient dopant is believed to have insignificant modification effect, whereas excessive dopant may result in reduction of the proportion of Ni or encasement of Ni active

sites [16].

According to Fig. 2, for all catalysts, toluene conversion increased with increasing temperature, which is due to that the reforming reaction is endothermic, and high temperature is conducive to the conversion of toluene. At 600 °C, 10Ni/MgAl have achieved toluene conversion of

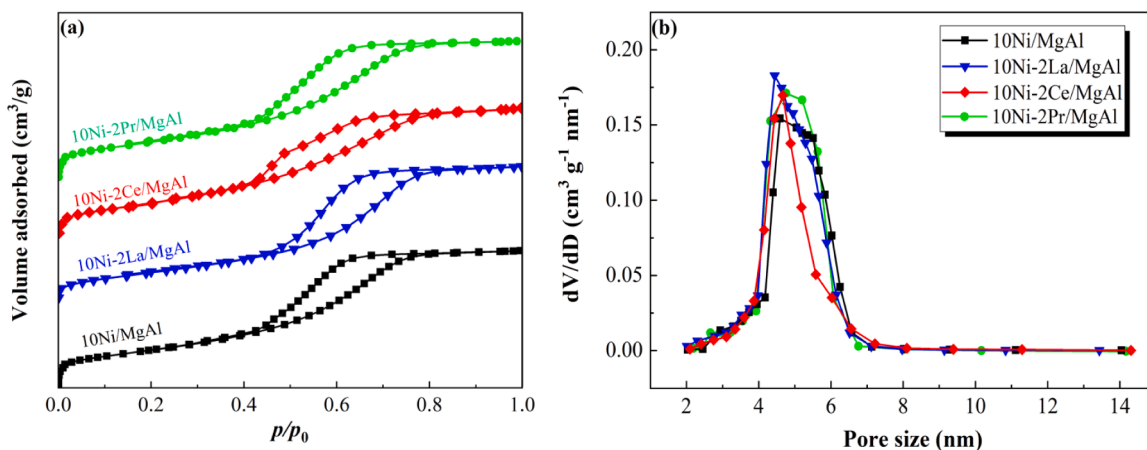


Fig. 3. (a) N_2 adsorption-desorption isotherms and (b) pore size distribution curves of the reduced catalysts.

94.9%. However, surprisingly, it could be observed that in case of the reforming temperature at 600 °C, except for La, the doping of the other two earth resulted in a slight decrease of toluene conversion. Possible reasons will be discussed in the DFT calculation later on. Based on these results, 10Ni/MgAl and the top-performing of 10Ni-2La/MgAl, 10Ni-2Ce/MgAl, and 10Ni-2Pr/MgAl were chosen for subsequent investigation.

3.2. Characterization analysis

3.2.1. Specific surface area and pore structure

According to Fig. 3a, each catalyst showed a type IV N_2 adsorption-desorption isotherm, suggesting their mesoporous structure [23]. In Fig. 3b, in contrast to 10Ni/MgAl, the amount of small-size pores (4–6 nm) increased in the three rare earth-doped samples, particularly in 10Ni-2La/MgAl which has more 4–5 nm pores. This result indicated that doping a small amount of rare earths might refine the pore structure of catalyst. The BET specific surface area and pore structure data are listed in Table 1. In comparison to 10Ni/MgAl, the three rare earth-doped catalysts exhibited a slightly larger specific surface area and pore volume, and a smaller most probable pore diameter.

3.2.2. XRD

As shown in the XRD patterns of the four catalysts (Fig. 4a), all the samples exhibited only diffraction peaks corresponding to $MgAl_2O_4$ spinel (PDF#21–1152) and metal Ni (PDF#04–0850), indicating that the rare earths were well dispersed in the catalyst. It could be observed that compared to 10Ni/MgAl, the diffraction peaks of both Ni and $MgAl_2O_4$ spinel in the rare earth-doped catalysts were broadened. Accordingly, as listed in Table 1, the grain size of $MgAl_2O_4$ (6.95–8.23 nm) and metal Ni (4.36–5.93 nm) in the rare earth-doped catalysts were smaller than those in 10Ni/MgAl. These results demonstrated that the doping of rare earths not only refined the support grain, but also promoted the dispersion of Ni, resulting in the formation of smaller Ni particles. Among the three rare earths, La dopant exhibited the most pronounced effect.

3.2.3. H_2 -TPR and CO_2 -TPD

The H_2 -TPR curves of four catalysts could be deconvoluted into two distinct reduction peaks (Fig. 5a). The peaks at low temperature (around 580 °C) were attributed to the reduction of bulk NiO, which had weak interaction with the support [25]. The peaks at high temperature (669–680 °C) were ascribed to the reduction of the highly dispersed NiO nanoparticles, which exhibited strong interaction with the support due to their large metal-support interface [25,26]. Compared to 10Ni/MgAl, all three doped samples exhibited a decreased proportion of low-temperature peaks and an increased share of high-temperature peaks to varying degrees. This confirmed that the rare earth doping led to improved dispersion of Ni species. Among the rare earth-doped catalysts, the La-modified sample was distinguished by a

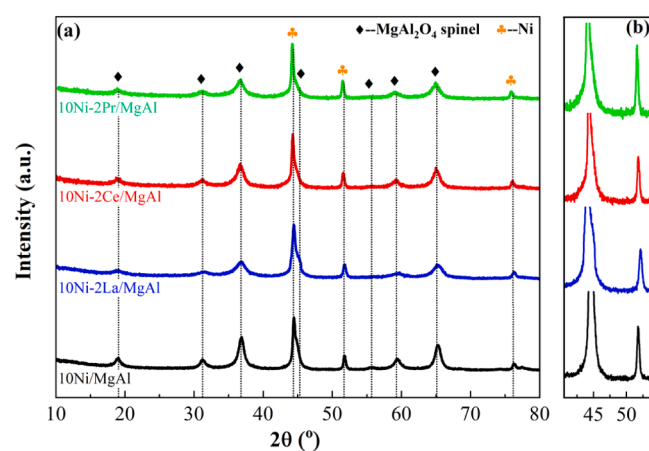


Fig. 4. (a) XRD patterns of the reduced four catalysts, (b) the enlarged patterns in scope of 40–53 °.

low-temperature peak area of only 1.8 and a high-temperature peak area of 10.5. Furthermore, it is noteworthy that the high-temperature peaks of the three rare earth-doped samples shifted to higher temperature (675–680 °C) compared to 10Ni/MgAl (669 °C), thus providing another evidence for the improved dispersion of NiO [26].

The rare earth dopants have been found to impact the alkalinity of the catalyst, which in turn affected its stability against carbon deposition [27]. In Fig. 5b, the CO_2 -TPD curves of four reduced catalysts are deconvoluted into three peaks, corresponding to the desorption of CO_2 at weak (95–100 °C), medium (150–200 °C), and strong (400–450 °C) alkaline sites, respectively [27]. The weak alkaline site was related to Brønsted base, while the medium and strong alkaline sites were linked to Lewis base (low coordination O^{2-} ion) [27]. According to the peak areas, the three rare earth doped samples showed a significant increase in medium and strong alkaline sites compared to 10Ni/MgAl. This might be explained as that the doping of rare earth resulted in larger specific surface area and smaller particle size of $MgAl_2O_4$, which enabled more exposure of low coordination O^{2-} [27]. It could be observed that 10Ni-2La/MgAl exhibited a much larger peak area (0.22) of strong alkaline site compared to Ce and Pr-doped samples (0.10 and 0.15). This might be due to La_2O_3 reacting with CO_2 to form $La_2O_2CO_3$, and the decomposition of $La_2O_2CO_3$ at this temperature contributing additional peak area [28]. $La_2O_2CO_3$ could remove the deposited carbon on the catalyst and increase CO production through reaction (3) [29].



In summary, the three rare earth dopants enhanced the alkalinity of Ni/ $MgAl_2O_4$, and, it could be predicted that the doping of La would improve the catalyst coke resistance.

3.2.4. XPS

XPS was employed to investigate the electron transfer between Ni and rare earth atoms. The XPS spectrum of Ni 2p (Fig. 6a) could be deconvoluted into three distinct peaks, corresponding to Ni^0 (851.3–852.3 eV), Ni^{2+} (855.3–855.5 eV), and a satellite peak (860–861 eV) [23]. The presence of Ni^{2+} was attributed to partial oxidation of samples during placement before testing. The binding energies of the Ni^0 peak in La-, Ce-, and Pr-doped samples were 851.4, 851.8, and 851.3 eV, respectively. These values were lower than that of 10Ni/MgAl (852.3 eV). The decrease in binding energy indicated an increase in valence electron density. Meanwhile, in Fig. 6b, c and d, it was noticed that the deconvoluted peaks of all the three rare earth elements shifted towards higher binding energy compared to the corresponding reported values in literature (indicated by the red line in the figure) [23,30–32]. These results substantiated that the La, Ce, and Pr dopants in the catalyst donated a portion of valence electron to Ni,

Table 1
Texture data of four catalyst samples.

Catalysts	S_{BET} (m^2/g) ^a	V_{tot} (cm^3/g) ^a	D_{pore} (nm) ^a	$MgAl_2O_4$ size (nm) ^b	Ni size (nm) ^b
10Ni/MgAl	148.88	0.24	6.09	9.24	6.10
10Ni-2La/ MgAl	156.63	0.26	5.96	6.95	4.36
10Ni-2Ce/ MgAl	151.09	0.25	6.01	8.23	5.93
10Ni-2Pr/ MgAl	152.60	0.26	5.97	8.18	5.87

^a BET specific surface area (S_{BET}), total pore volume (V_{tot}) and the most probable pore diameter (D_{pore}) determined by N_2 adsorption-desorption isotherm;

^b Crystalline size calculated by Scherrer's equation according to XRD patterns.

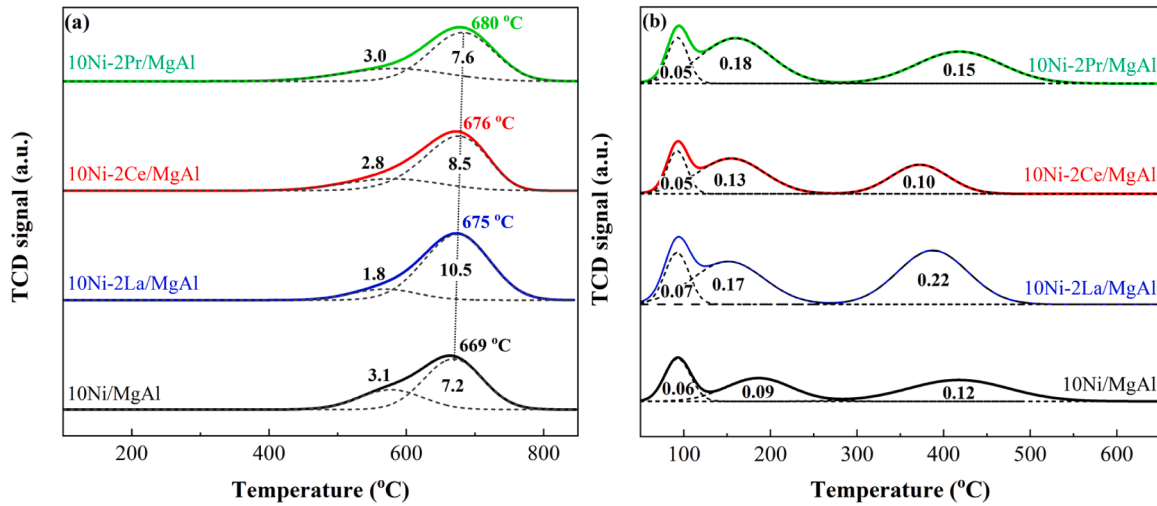


Fig. 5. (a) $\text{H}_2\text{-TPR}$ and (b) $\text{CO}_2\text{-TPD}$ profiles of four catalysts.

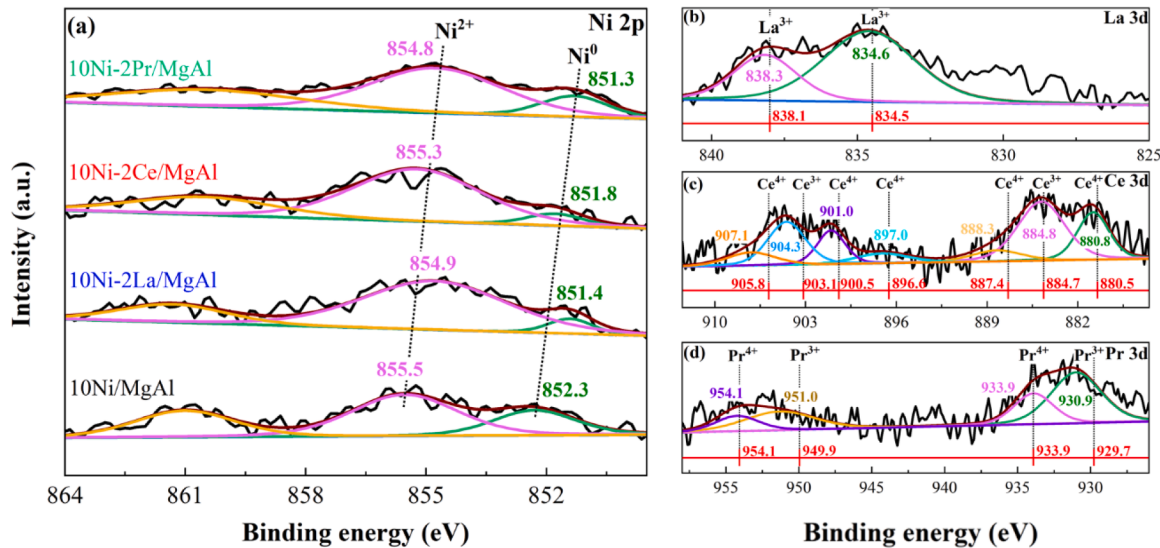


Fig. 6. XPS spectra of (a) Ni 2p, (b) La 3d, (c) Ce 3d, (d) Pr 3d of the four reduced catalysts.

augmenting its valence electron density. Higher valence electron density suggested stronger capacity of Ni for adsorption and activation of the organic solvent molecules [21,22].

Based on the current characterization results, it could be confirmed that rare earth dopants not only optimized the texture properties and basicity of the support, but also promoted Ni dispersion. The XPS results further confirmed the occurrence of electron transfer from rare earth atoms and to Ni, indicating that the electronic structure of Ni was also modulated. In the subsequent analysis, this phenomenon will be investigated from a theoretical calculation perspective.

3.3. DFT calculations

3.3.1. Effect of rare earth dopants on Ni electronic structure

The $\text{Ni}/\text{MgAl}_2\text{O}_4$ catalyst model was constructed by placing a Ni cluster on the surface of MgAl_2O_4 spinel, and its optimized structure is depicted in Fig. 7a. The doping models were constructed through replacing a Ni atom with a La, Ce or Pr atom respectively in the lower right corner of Ni_4 clusters, which are illustrated in Fig. 7b, c and d. (top view). Through Bader charge population analysis, the number of electrons in Ni's valence orbitals (3d and 4 s) were obtained and are shown

as the main view. As it can be observed, the introduction of rare earth atoms increases the valence electron count of Ni clusters, and the Ni cluster doped with La exhibits the maximum number of valence electron (10.4 e, 9.7 e, 9.6 e) of the three Ni atoms. Additionally, the charge density difference (Fig. S2) illustrates the electrons transfer process from rare earth atoms to Ni clusters, which leads to the increase in valence electron in Ni atoms. Overall, the DFT calculation results are consistent with those observed in XPS spectra.

Electron transfer between Ni clusters and rare earth atoms may arise from their orbital interactions. Thus, the projected density of states (pDOS) of Ni clusters and rare earth atoms in each model was analyzed. In Fig. 7, only the pDOS of Ni 3d and rare earth 5d orbitals are presented, as their other valence orbitals do not exhibit significant interaction (not shown). As shown in Fig. 7b, c, d, the pDOS peaks of Ni 3d orbitals have significant resonance with that of 5d orbitals of La, Ce or Pr atoms in scope of 1–7 eV, indicating their strong interaction.

In the pDOS diagrams, it could be observed that the occupied states of Ni 3d orbitals (i.e., pDOS peaks below the Fermi level) of the three doping models are more densely concentrated in a higher energy range. For instance, the most conspicuous one is the La-doped model (Fig. 7b), in which the pDOS peak of Ni 3d occupied state is predominantly

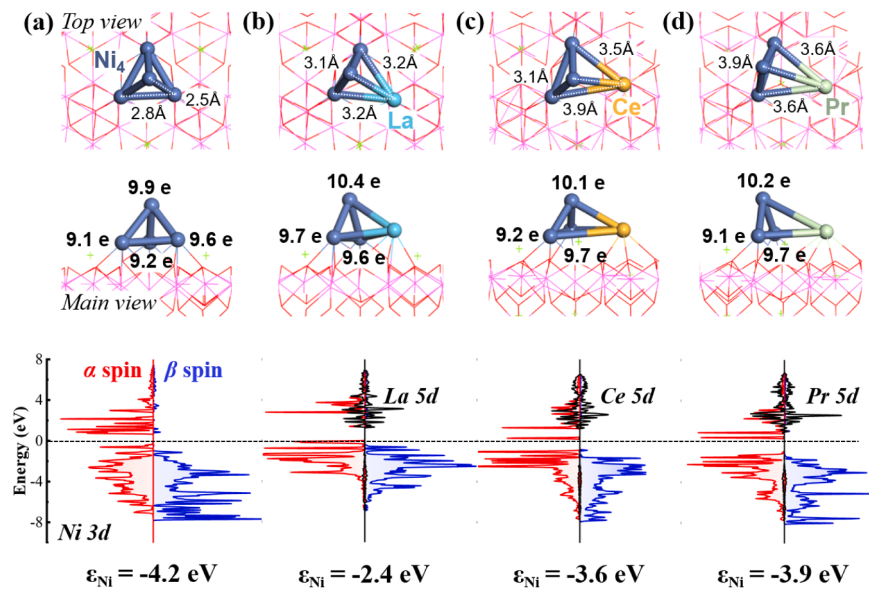


Fig. 7. The structure optimized models of (a) Ni/MgAl, (b) Ni-La/MgAl, (c) Ni-Ce/MgAl, (d) Ni-Pr/MgAl (the display style of MgAl₂O₄ substrate is line); below the models are the pDOS diagrams of Ni cluster (red and blue curves) and rare earth atoms (black curves) corresponding to each model (dash line: Fermi energy).

concentrated at $-5\text{--}0$ eV, significantly higher than that of undoped Ni₄ cluster (peaks dispersed within -8 to 0 eV, Fig. 7a). The d-band center (ϵ_{Ni}) of the occupied Ni 3d orbital for each model was calculated (Fig. 7). The ϵ_{Ni} of Ni cluster (-2.4 eV) doped with La is significantly higher than that of Ni clusters doped with Ce and Pr (-3.6 and -3.9 eV), while the undoped Ni₄ cluster has the lowest ϵ_{Ni} (-4.2 eV). This result suggests that the ϵ_{Ni} of Ni can be enhanced by rare earth dopants via their orbital interaction, with La dopant exhibiting the most pronounced effect. According to the theory of d-band center, for a Ni atom, a higher value of ϵ_{Ni} suggests a greater electron donation capacity, thereby, this Ni has higher ability to adsorb organic molecules and activate the corresponding bonds [33].

3.3.2. Account of the doping effect of La stronger than that of Ce and Pr

The aforementioned theoretical calculations demonstrated that rare earth dopants could enhance both valence electron density and ϵ_{Ni} of Ni. However, a persistent query remains that despite the three lanthanide dopants sharing similar chemical properties, why La exerts a

significantly stronger influence on promoting the electronic properties of Ni than Ce and Pr. From the bond length data in Fig. 7 (top view), this may be due to Ce and Pr being far away from the Ni atom, resulting in weaker orbital interaction with Ni. In other words, Ce- and Pr-doped Ni clusters are structural instability, with Ce and Pr atoms being repelled. This behavior differs from that observed in La-doped model (Fig. 7b). The stability of these three doping models was further investigated through AIMD simulations at 550 °C for 10 ps (Please refer to [Supplementary Materials](#) for AIMD trajectory animation). After the 10 ps AIMD process, the La-Ni cluster structure (Fig. 8a) remains stable, whereas the Ce-Ni and Pr-Ni cluster structures (Fig. 8b, c) experience collapse. The radial distribution function (Fig. 8d) indicates that during the AIMD process, the distribution density of Ni atoms around La in La-Ni cluster is significantly higher than that in Ce-Ni and Pr-Ni clusters below 4 Å, indicating a greater average distance between Ni atoms and Ce or Pr atom. According to the aforementioned results, it can be inferred that La and Ni clusters possess favorable "compatibility" and are capable of forming a stable La-Ni structure. The poor compatibility of Ce or Pr

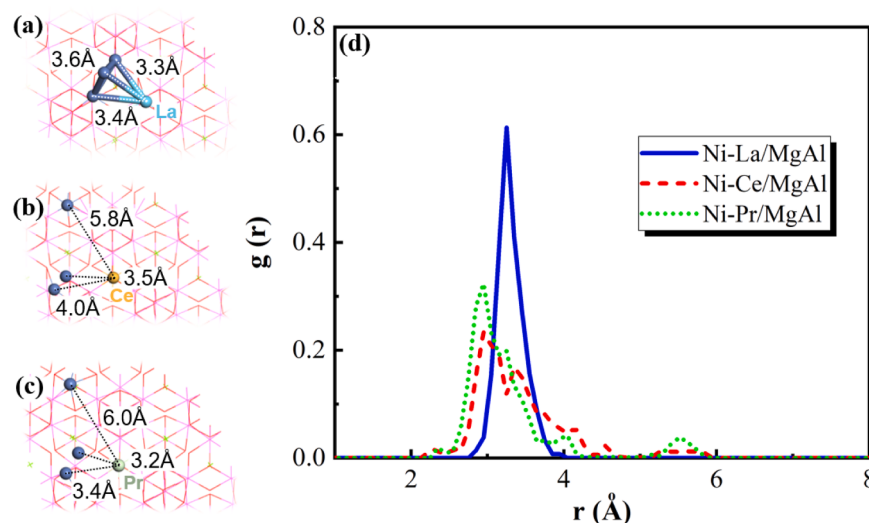


Fig. 8. The simulated equilibrium structures of (a) Ni-La/MgAl, (b) Ni-Ce/MgAl, (c) Ni-Pr/MgAl after AIMD runs at 550 °C for 10 ps; (d) the radial distribution function ($g(r)$) of Ni atoms around the rare earth atom in each model.

dopant with Ni may lead to their segregation from the Ni component. Consequently, as demonstrated by XRD and H₂-TPR, the promotion of Ni dispersion by Ce and Pr dopants was not as good as that by La. In addition, AIMD simulation result might explain the phenomenon that 10Ni/MgAl even achieved higher toluene conversion than 10Ni-2Ce/MgAl and 10Ni-2Pr/MgAl. That was due to the instability of Ce-Ni and Pr-Ni clusters at high temperatures (higher than 550 °C).

3.3.3. The origin of the compatibility between La dopant and Ni cluster

To investigate the origin of the compatibility between La and Ni cluster, the spin-polarized density of the three doping models were compared. As shown in Fig. 9, Ce and Pr atoms exhibit spin polarization (represented by the yellow electron cloud), with spin magnetizations of 0.99 and 2.01 μ_B , respectively. As depicted in the pDOS diagrams below, the spin polarization of Ce and Pr originates from their unpaired β electrons in 4 f orbitals (indicated by arrows), while La 4 f orbital exhibits negligible spin polarization (with magnetization of only 0.02 μ_B) due to the absence of unpaired 4 f electrons. Furthermore, Ce and Pr atoms also induce an increase in the spin magnetization of the surrounding Ni atoms (compared to the La doping model). Hence, the high spin polarization of Ce-Ni and Pr-Ni clusters is speculated to be responsible for their structural instability. This can be attributed to the fact that a high spin state, i.e. more unpaired electrons, is unfavorable for energy minimization of the system [34]. In other words, the compatibility between La and Ni cluster may be attributed to the low spin polarization of La-Ni structure.

3.4. Catalytic steam reforming tests

The steam reforming experiments were carried out on four catalysts using various volatile organic solvents, including toluene, acetone, tetrahydrofuran and n-hexane, as illustrated in Fig. 10. Overall, in terms of solvent conversion efficiency (curve, left Y-axis), rare earth-doped Ni/MgAl₂O₄ exhibited a better performance than undoped Ni/MgAl₂O₄ in 500–550 °C. Among them, the La-doped catalyst exhibited notably superior performance compared to Ce and Pr-doped ones, particularly at low temperatures. For example, at 500 °C, the toluene reforming conversion efficiency over 10Ni-2La/MgAl (Fig. 10a) reached up to 92.8%, whereas that of Ce and Pr-doped samples was only approximately 67–68% and that of 10Ni/MgAl was merely 48.1%. Besides, the 10Ni-2La/MgAl catalyst also exhibited excellent low-temperature conversion efficiency for acetone (96.2%), tetrahydrofuran (94.1%), and n-hexane (97.5%) at 500 °C. Combined with characterizations and theoretical calculations, the superior performance of 10Ni-2La/MgAl catalyst can be attributed to the significant modification of La dopant on the

dispersion and electronic properties (increasing valence electron density and d-band center) of Ni component. The modulation of Ni electronic properties is likely the crucial factor, as it enhanced the capacity of Ni to adsorb organic solvent molecules and activate C-C/C-H/C-O bonds from the source. Similarly, Joo et al. found that the incorporation of Fe led to a 0.3 eV increase in the d-band center of CoNiFe catalyst, resulting in an almost 15% enhancement in methane dry reforming conversion efficiency [33].

As shown in Fig. 10 (column, right Y-axis), the reforming products of solvents consists of H₂, CH₄, CO, and CO₂. Compared to the other three catalysts, 10Ni-2La/MgAl exhibited a consistently lower selectivity towards CO₂ across all solvents. This might be attributed to the strong adsorption of CO₂ by La₂O₃ (forming La₂O₂CO₃). Consequently, a greater proportion of combustible gas (H₂, CH₄, CO) was produced on 10Ni-2La/MgAl catalyst. Besides, 10Ni-2La/MgAl also exhibited a more pronounced CH₄ production, especially at low temperature. Based on the correlation between methane production and temperature, it was postulated that CH₄ was generated through CO₂ methanation (reaction (4), $\Delta H_{298} = -165 \text{ kJ/mol}$). La₂O₂CO₃ served as a reactant reservoir to facilitate this process [35].



As the LHV of CH₄ is higher than that of H₂ and CO [7], and based on the aforementioned results, it can be inferred that 10Ni-2La/MgAl catalyst would exhibit a higher power output per unit of solvent owing to its higher fuel and methane selectivity. Notably, the proportion of CO in reforming products derived from 10Ni-2La/MgAl was significantly greater than that observed in other samples. This could be attributed to the reaction between La₂O₂CO₃ and the carbon species deposited during stream reforming (reaction (3)), which portends that this catalyst has remarkable coking resistance.

3.5. Steam reforming of the mixed solvent

By utilizing four-solvent mixtures as the recovered volatile organic solvent model, a 10-hour continuous steam reforming experiment at 550 °C was conducted on 10Ni-2La/MgAl. As shown in Fig. 11a, 10Ni-2La/MgAl demonstrated an average conversion efficiency of 97.3% towards the mixed solvent, and maintained its stability throughout the testing period. Compared with the previous 3DOM Ni-Pt/Ce_{0.8}Zr_{0.2}O₂ and other reported catalysts (Table S2), the 10Ni-2La/MgAl shows exceeding catalytic activity and carbon deposition resistance even at a lower temperature. Stable production of gas fuel could be also observed in Fig. 11a, and the average yields of H₂, CH₄, CO was 2.7, 0.05 and 0.45 mmol/min, respectively. According to the LHV of H₂ (143 MJ/kg),

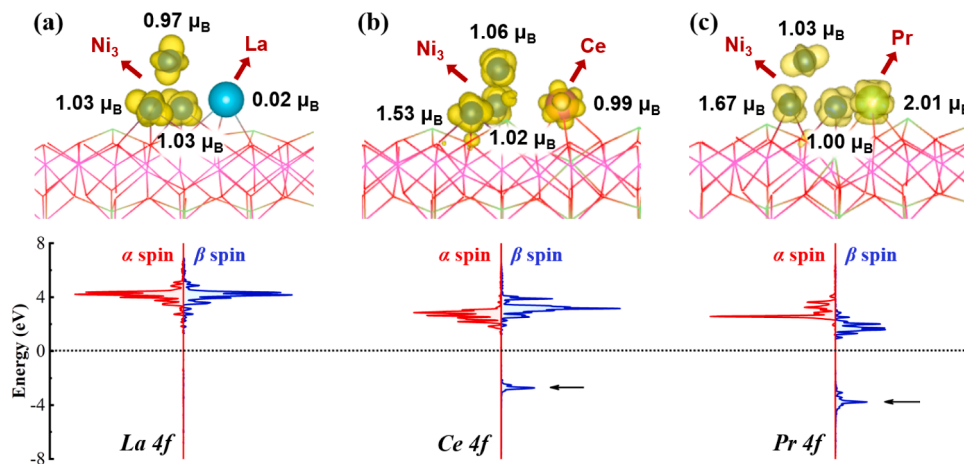


Fig. 9. The spin polarized charge density of (a) Ni-La/MgAl, (b) Ni-Ce/MgAl, (c) Ni-Pr/MgAl (the yellow electron cloud corresponds spin up; the number represents spin magnetization); below the model are the pDOS diagrams of La 4 f, Ce 4 f and Pr 4 f (dash line: Fermi energy).

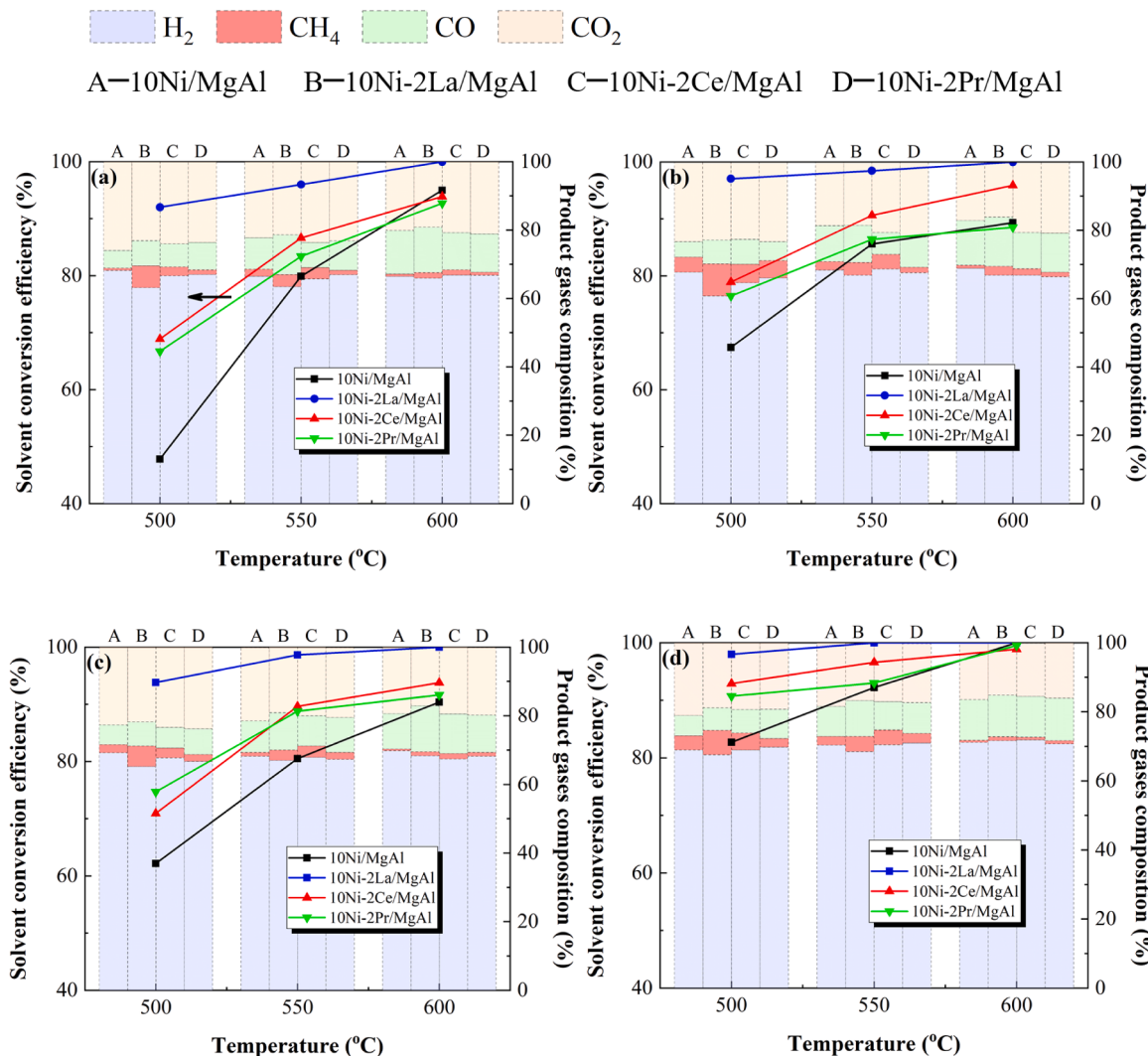


Fig. 10. Steam reforming activity (curves, left Y-axis) and product gas composition (column, right Y-axis) of (a) toluene, (b) acetone, (c) tetrahydrofuran, (d) n-hexane over four catalysts.

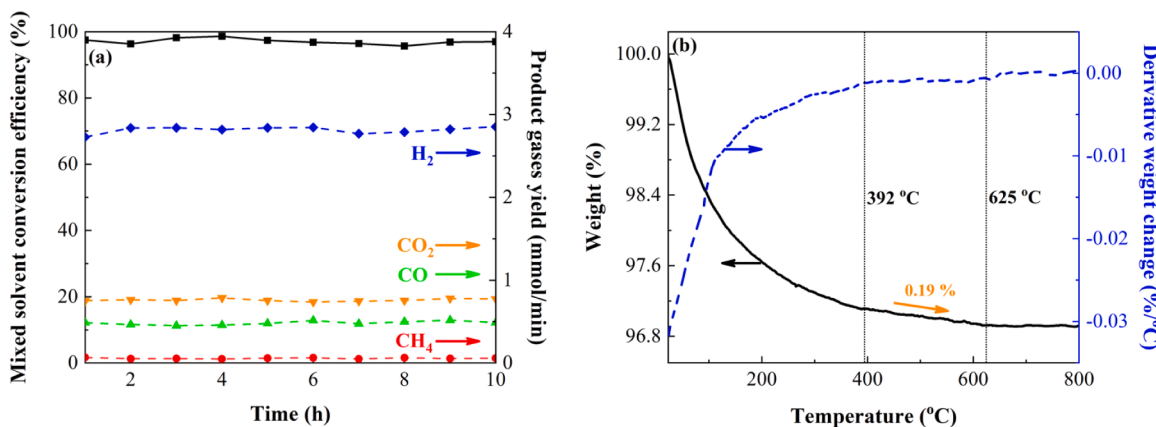


Fig. 11. (a) 10-hour steam reforming of the mixed solvent on 10Ni-2La/MgAl (reaction temperature: 550 °C), (b) TGA characterization on 10Ni-2La/MgAl after 10-hour operation.

CH_4 (50 MJ/kg) and CO (10 MJ/kg), and their respective mass fractions in the producer gas, the average LHV of the producer gas fuel (Including the carrier gas N_2) was calculated as 4.92 MJ/kg (i.e. 4.39 MJ/m³) meeting the LHV requirement of fuel gas for ICE power generation

(3.0–5.6 MJ/m³) [7]. The 10Ni-2La/MgAl subjected to a 10-hour test was used for TGA, as depicted in Fig. 11b. A two-stage weight loss process could be distinguished in TGA curve, which was attributed to water desorption (≤ 392 °C) and insignificant coke combustion

(392–625 °C) [23]. Based on the combustion temperature, the coke was attributed to amorphous carbon [23]. The combustion of amorphous carbon resulted in a weight loss of 0.19 wt% (Fig. 11b) and the carbon deposition rate was calculated to be 2.9 mg/(h·g_{catalyst}). As presented in Table S2, it is significantly lower than that of other reported catalysts. As previously discussed, this can be attributed to the characteristic of La₂O₃CO₃ removing carbon species (reaction (3)). The exceptional resistance to coking displayed by 10Ni-2La/MgAl indicated that this catalyst holds promise for stable operation in industrial applications.

4. Conclusions

To develop a steam reforming catalyst, that is efficient and durable in relatively low temperatures, and is applicable to various volatile organic solvents with different structures, Ni/MgAl₂O₄ catalysts doped with three rare earths, La, Ce, and Pr, were synthesized via a novel one-step sol-gel preparation method. The characterization results combined with DFT calculations revealed that the doping of the three rare earths not only improved the catalyst structure, but also promoted Ni dispersion and increased its valence electron density and d-band center. Among them, low-spin La dopants exhibit unique structural compatibility with Ni clusters, resulting in a more pronounced modification effect on Ni. Consequently, in steam reforming of various volatile organic solvents, the catalytic activity follows: 10Ni-2La/MgAl > > 10Ni-2Ce/MgAl ~ 10Ni-2Pr/MgAl > 10Ni/MgAl in 500–550 °C. By utilizing mixtures of toluene, acetone, tetrahydrofuran, n-hexane with a molar ratio of 1:1:1:1 as a model of industrial recovered volatile organic solvents, the 10Ni-2La/MgAl catalyst demonstrated an impressive average steam reforming conversion efficiency of 97.3%, and carbon deposition rate of only 2.9 mg/(h·g_{catalyst}) over ten hours of operation at 550 °C. Due to its excellent low-temperature activity and coking resistance, wide adaptability, ease of preparation, and cost-effectiveness, 10Ni-2La/MgAl exhibits great potential as a steam reforming catalyst for converting recovered volatile organic solvents into gas fuel for power generation in practical engineering.

CRediT authorship contribution statement

Feng Lin: Conceptualization, Data curation, Formal analysis, Investigation, Methodology, Resources, Software, Visualization, Writing – original draft, Writing – review & editing. **Xiangwei Ma:** Data curation, Investigation, Methodology. **Zezhi Chen:** Methodology, Resources, Writing – review & editing, Supervision. **Huijuan Gong:** Methodology, Resources, Writing – review & editing, Supervision. **Mingze Xu:** Data curation, Investigation, Methodology.

Declaration of Competing Interest

The authors declare that they have no known competing financial interests or personal relationships that could have appeared to influence the work reported in this paper.

Data Availability

No data was used for the research described in the article.

Acknowledgments

The authors gratefully acknowledge the financial supports from the National Natural Science Foundation of China (No. 22076077, 21577060), Jiangsu Science and Technology Department (BK 20191256).

Appendix A. Supporting information

Supplementary data associated with this article can be found in the

online version at doi:10.1016/j.apcatb.2023.123212.

References

- [1] C.J. Clarke, W. Tu, O. Levers, A. Brohl, J.P. Hallett, Green and sustainable solvents in chemical processes, *Chem. Rev.* 118 (2018) 747–800, <https://doi.org/10.1021/acs.chemrev.7b00571>.
- [2] H. Wang, S. Sun, L. Nie, Z. Zhang, W. Li, Z. Hao, A review of whole-process control of industrial volatile organic compounds in China, *J. Environ. Sci.* 123 (2023) 127–139, <https://doi.org/10.1016/j.jes.2022.02.037>.
- [3] C. Duan, H. Liao, K. Wang, Y. Ren, The research hotspots and trends of volatile organic compound emissions from anthropogenic and natural sources: a systematic quantitative review, *Environ. Res.* 216 (2023), 114386, <https://doi.org/10.1016/j.envres.2022.114386>.
- [4] B. Liu, J. Ji, B. Zhang, W. Huang, Y. Gan, D.Y.C. Leung, H. Huang, Catalytic ozonation of VOCs at low temperature: a comprehensive review, *J. Hazard. Mater.* 422 (2022), 126847, <https://doi.org/10.1016/j.jhazmat.2021.126847>.
- [5] S. Yuan, W. Yang, H. Yin, Z. Chen, Separation of acetone–tetrahydrofuran azeotropic mixture by continuous extractive distillation, *J. Chem. Technol. Biot.* 88 (2013) 1523–1528, <https://doi.org/10.1002/jctb.3997>.
- [6] D. Constable, C. Gonzalez, R.K. Henderson, Perspective on solvent use in the pharmaceutical industry, *Org. Process Res. Dev.* 11 (2007) 133–137, <https://doi.org/10.1021/op060170h>.
- [7] Y. Zhou, X. Ma, Z. Chen, H. Gong, L. Chen, H. Yu, Study on the feasibility of converting the recovered volatile organic compounds to syngas via catalytic steam reforming for gas-fueled power generation, *Energy* 263 (2023), 125761, <https://doi.org/10.1016/j.energy.2022.125761>.
- [8] S. Zhou, Z. Chen, H. Gong, X. Wang, T. Zhu, Y. Zhou, Low-temperature catalytic steam reforming of toluene as a biomass tar model compound over three-dimensional ordered macroporous Ni-Pt/Ce_{1-x}Zr_xO₂ catalysts, *Appl. Catal. A: Gen.* 607 (2020), 117859, <https://doi.org/10.1016/j.apcata.2020.117859>.
- [9] L.V. Mattos, G. Jacobs, B.H. Davis, F.B. Noronha, Production of hydrogen from ethanol: review of reaction mechanism and catalyst deactivation, *Chem. Rev.* 112 (2012) 4094–4123, <https://doi.org/10.1021/cr2000114>.
- [10] Y. Wang, X. Yang, Y. Wang, Catalytic performance of mesoporous MgO supported Ni catalyst in steam reforming of model compounds of biomass fermentation for hydrogen production, *Int. J. Hydrol. Energ.* 41 (2016) 17846–17857, <https://doi.org/10.1016/j.ijhydene.2016.07.258>.
- [11] J. Li, X. Mei, L. Zhang, Z. Yu, Q. Liu, T. Wei, W. Wu, D. Dong, L. Xu, X. Hu, A comparative study of catalytic behaviors of Mn, Fe, Co, Ni, Cu and Zn-Based catalysts in steam reforming of methanol, acetic acid and acetone, *Int. J. Hydrol. Energ.* 45 (2020) 3815–3832, <https://doi.org/10.1016/j.ijhydene.2019.03.269>.
- [12] A. Dehghanpoor-Gharashah, M. Rezaei, F. Meshkani, Preparation and improvement of the mesoporous nanostructured nickel catalysts supported on magnesium aluminate for syngas production by glycerol dry reforming, *Int. J. Hydrol. Energ.* 46 (2021) 22454–22462, <https://doi.org/10.1016/j.ijhydene.2021.04.072>.
- [13] K. Takehira, T. Shishido, P. Wang, T. Kosaka, K. Takaki, Autothermal reforming of CH₄ over supported Ni catalysts prepared from Mg-Al hydroalumite-like anionic clay, *J. Catal.* 221 (2004) 43–54, <https://doi.org/10.1016/j.jcat.2003.07.001>.
- [14] R. Trane-Restrup, S. Dahl, A.D. Jensen, Steam reforming of ethanol over Ni-based catalysts: effect of feed composition on catalyst stability, *Int. J. Hydrol. Energ.* 39 (2014) 7735–7746, <https://doi.org/10.1016/j.ijhydene.2014.03.107>.
- [15] T. Zhu, Z. Chen, H. Gong, H. Yu, P. Ning, S. Zhou, Y. Zhou, Seeded-growth preparation of high-performance Ni/MgAl₂O₄ catalysts for tar steam reforming, *N. J. Chem.* 44 (2020) 13692–13700, <https://doi.org/10.1039/donj01468k>.
- [16] A.A. Fard, R. Arvaneh, S.M. Alavi, A. Bazyari, A. Valaei, Propane steam reforming over promoted Ni-Ce/MgAl₂O₄ catalysts: effects of Ce promoter on the catalyst performance using developed CCD model, *Int. J. Hydrol. Energ.* 44 (2019) 21607–21622, <https://doi.org/10.1016/j.ijhydene.2019.06.100>.
- [17] J.E. Park, K.Y. Koo, U.H. Jung, J.H. Lee, H. Roh, W.L. Yoon, Syngas production by combined steam and CO₂ reforming of coke oven gas over highly sinter-stable La-promoted Ni/MgAl₂O₄ catalyst, *Int. J. Hydrol. Energ.* 40 (2015) 13909–13917, <https://doi.org/10.1016/j.ijhydene.2015.08.026>.
- [18] S.K. Malik, F.J. Arlinghaus, W.E. Wallace, Calculation of the spin-polarized energy-band structure of LaNi₅ and GdNi₅, *Phys. Rev. B* 25 (1982) 6488–6491, <https://doi.org/10.1103/PhysRevB.25.6488>.
- [19] H. Zheng, Y. Wang, G. Ma, Electronic structure of LaNi₅ and its hydride LaNi₅H₇, *Eur. Phys. J. B* 29 (2002) 61–69, <https://doi.org/10.1140/epjb/e2002-00262-2>.
- [20] H. Li, J. Ren, X. Qin, Z. Qin, J. Lin, Z. Li, Ni/SBA-15 catalysts for CO methanation: effects of V, Ce, and Zr promoters, *RSC Adv.* 5 (2015) 96504–96517, <https://doi.org/10.1039/c5ra15990c>.
- [21] M. Li, Z. Lu, G. Wang, The effect of potassium on steam-methane reforming on the Ni₄/Al₂O₃ surface: a DFT study, *Catal. Sci. Technol.* 7 (2017) 3613–3625, <https://doi.org/10.1039/c7cy00986k>.
- [22] H. Liu, B. Teng, M. Fan, B. Wang, Y. Zhang, H.G. Harris, CH₄ dissociation on the perfect and defective MgO(001) supported Ni₄, *Fuel* 123 (2014) 285–292, <https://doi.org/10.1016/j.fuel.2014.01.087>.
- [23] F. Lin, Z. Chen, H. Gong, X. Wang, L. Chen, H. Yu, Oxygen vacancy induced strong metal-support interactions on Ni/Ce_{0.8}Zr_{0.2}O₂ nanorod catalysts for promoting steam reforming of toluene: experimental and computational studies, *Langmuir* 39 (2023) 4495–4506, <https://doi.org/10.1021/acs.langmuir.3c00195>.
- [24] Z. Dong, T. Xia, Q. Li, J. Wang, S. Li, L. Sun, L. Huo, H. Zhao, Addressing the origin of highly catalytic activity of A-site Sr-doped perovskite cathodes for intermediate-

- temperature solid oxide fuel cells, *Electrochim. Commun.* 140 (2022), 107341, <https://doi.org/10.1016/j.elecom.2022.107341>.
- [25] A.H. Khoja, M. Tahir, N.A.S. Amin, Evaluating the performance of a Ni catalyst supported on $\text{La}_2\text{O}_3\text{-MgAl}_2\text{O}_4$ for dry reforming of methane in a packed bed dielectric barrier discharge plasma reactor, *Energy Fuels* 33 (2019) 11630–11647, <https://doi.org/10.1021/acs.energyfuels.9b02236>.
- [26] J. Guo, H. Lou, H. Zhao, D. Chai, X. Zheng, Dry reforming of methane over nickel catalysts supported on magnesium aluminate spinels, *Appl. Catal. A: Gen.* 273 (2004) 75–82, <https://doi.org/10.1016/j.apcata.2004.06.014>.
- [27] J. Ni, B. Jing, J. Lin, B. Lin, Z. Zhao, L. Jiang, Effect of rare earth on the performance of Ru/MgAl-LDO catalysts for ammonia synthesis, *J. Rare Earth* 36 (2018) 135–141, <https://doi.org/10.1016/j.jre.2017.07.011>.
- [28] Z. Huang, B. Liu, X. Tang, X. Wang, R. Amin, Performance of rare earth oxide doped Mn-based sorbent on various silica supports for hot coal gas desulfurization, *Fuel* 177 (2016) 217–225, <https://doi.org/10.1016/j.fuel.2016.03.009>.
- [29] N. Gao, J. Salisu, C. Quan, P. Williams, Modified nickel-based catalysts for improved steam reforming of biomass tar: a critical review, *Renew. Sust. Energy Rev.* 145 (2021), 111023, <https://doi.org/10.1016/j.rser.2021.111023>.
- [30] P. Mierczynski, M. Mosinska, N. Stepinska, K. Chalupka, M. Nowosielska, W. Maniukiewicz, J. Rogowski, N. Goswami, K. Vasilev, M.I. Szynkowska, Effect of the support composition on catalytic and physicochemical properties of Ni catalysts in oxy-steam reforming of methane, *Catal. Today* 364 (2021) 46–60, <https://doi.org/10.1016/j.cattod.2020.05.037>.
- [31] J. Lu, Y. Lei, G. Wan, Z. Mei, J. Yu, Y. Zhao, S. He, Y. Luo, Weakening the metal-support strong interaction to enhance catalytic performances of alumina supported Ni-based catalysts for producing hydrogen, *Appl. Catal. B: Environ.* 263 (2020), 118177, <https://doi.org/10.1016/j.apcatb.2019.118177>.
- [32] R. Zhou, R. Zhou, D. Alam, T. Zhang, W. Li, Y. Xia, A. Mai-Prochnow, H.J. An, E. C. Lovell, H. Masood, R. Amal, K. Ostrikov, P.J. Cullen, Plasmacatalytic bubbles using CeO_2 for organic pollutant degradation, *Chem. Eng. J.* 403 (2021), 126413, <https://doi.org/10.1016/j.cej.2020.126413>.
- [33] S. Joo, K. Kim, O. Kwon, J. Oh, H.J. Kim, L. Zhang, J. Zhou, J. Wang, H.Y. Jeong, J. Han, G. Kim, Enhancing thermocatalytic activities by upshifting the d-band center of exsolved Co-Ni-Fe ternary alloy nanoparticles for the dry reforming of methane, *Angew. Chem. Int. Ed.* 60 (2021) 15912–15919, <https://doi.org/10.1002/anie.202101335>.
- [34] D. Meng, Z. Zhu, G. Jiang, Geometrical configurations of Pu_4 and the Jahn-Teller effect, *J. Mol. Struct.* 610 (2002) 241–245, [https://doi.org/10.1016/S0022-2860\(02\)00043-1](https://doi.org/10.1016/S0022-2860(02)00043-1).
- [35] G. Garbarino, C. Wang, T. Cavattoni, E. Finocchio, P. Riani, M. Flytzani-Stephanopoulos, G. Busca, A study of Ni/ $\text{La-Al}_2\text{O}_3$ catalysts: a competitive system for CO_2 methanation, *Appl. Catal. B: Environ.* 248 (2019) 286–297, <https://doi.org/10.1016/j.apcatb.2018.12.063>.